Journal of Magnetic Resonance 223 (2012) 228–236

Contents lists available at SciVerse ScienceDirect

Journal of Magnetic Resonance

journal homepage: www.elsevier.com/locate/jmr

Uniform broadband excitation of crystallites in rotating solids using interleaved sequences of delays alternating with nutation

Veronika Vitzthum [a,*], Marc A. Caporini [a], Simone Ulzega [a,1], Julien Trébosc [b], Olivier Lafon [b], Jean-Paul Amoureux [b], Geoffrey Bodenhausen [a,c,d,e]

[a] Institut des Sciences et Ingénierie Chimiques (ISIC), Ecole Polytechnique Fédérale de Lausanne, 1015 Lausanne, Switzerland
[b] Unité de Catalyse et de Chimie du Solide (UCCS), CNRS 8181, University of Lille North of France, 59652 Villeneuve d'Ascq, France
[c] Département de Chimie, Ecole Normale Supérieure, 24 rue Lhomond, 75005 Paris, France
[d] Université Pierre et Marie Curie, Paris, France
[e] CNRS, UMR 7203, Paris, France

ARTICLE INFO

Article history:
Received 19 December 2011
Revised 24 April 2012
Available online 13 June 2012

Keywords:
Nitrogen-14 NMR
Delays Alternating with Nutations for Tailored Excitation (DANTE)
Interleaved DANTE
Dipolar Heteronuclear Multiple-Quantum Correlation (*D*-HMQC)
Solid-state NMR
Magic Angle Spinning (MAS)
Broadband excitation
Quadrupolar nuclei

ABSTRACT

In solids that are spinning about the magic angle, trains of short pulses in the manner of Delays Alternating with Nutations for Tailored Excitation (DANTE) allow one to improve the efficiency of the excitation of magnetization compared to rectangular pulses. By interleaving N pulse trains with $N > 1$, one obtains 'DANTE–N' sequences comprising N pulses per rotor period that extend over K rotor periods. Optimized interleaved DANTE schemes with $N > 1$ are shorter than basic DANTE-1 sequences with $N = 1$. Therefore, they are less affected by coherent or incoherent decays, thus leading to higher signal intensities than can be obtained with basic DANTE-1 or with rectangular pulses. Furthermore, the shorter length of DANTE-N with $N > 1$ increases the width of the spikelets in the excitation profile, allowing one to cover the range of isotropic chemical shifts and second-order quadrupolar effects typical for side-chain and backbone amide ^{14}N sites in peptides at $B_0 = 18.8$ T. In DANTE-N, spinning sidebands only appear at multiples of the spinning frequency ν_{rot}, as if the samples were rotating at $N\nu_{rot}$. We show applications to direct detection of nitrogen-14 nuclei with spin $I = 1$ subject to large quadrupole interactions, using fast magic angle spinning (typically $\nu_{rot} \geqslant 60$ kHz), backed up by simulations that provide insight into the properties of basic and interleaved DANTE sequences. When used for indirect detection, we show by numerical simulations that even basic DANTE-1 sequences can lead to a four-fold boost of efficiency compared to standard rectangular pulses.

1. Introduction

In static solids, nuclear magnetic resonance (NMR) spectra are often very broad, particularly for quadrupolar nuclei with $I > ½$, and for spins with $I = ½$ in paramagnetic samples. In the early days of continuous-wave excitation, it was straightforward to sweep the radio-frequency (*rf*) carrier over large bandwidths, and the main challenge of broad spectra arose from the weakness of signals that were spread over wide ranges of frequencies. Although the advent of pulsed excitation and Fourier transformation (FT) [1] heralded decisive advantages for spectra with bandwidths $\Delta\omega$ that are comparable with typical *rf* intensities ω_1, pulsed excitation is challenging for spectra with larger bandwidths. Various approaches to broadband excitation have been reviewed recently by Shurko et al. [2] with particular emphasis on ^{14}N spectra of static solids. Broadband excitation may benefit from pulses with very short durations τ_p that can cover large bandwidths $\Delta\omega \approx 2\pi/\tau_p$, although this usually entails small flip angles $\beta = |\gamma B_1 \tau_p| << \pi/2$, and hence poor S/N ratios, since the *rf* intensities are necessarily limited. Broadband excitation may be improved by recording complementary spectra in (possibly overlapping) segments.

On the other hand, narrow-band excitation can be achieved either by using weak *rf* amplitudes, or equivalently by applying long trains of intense short pulses at regular intervals τ_d. This type of excitation, dubbed Delays Alternating with Nutations for Tailored Excitation (DANTE) [3], has become popular for selective excitation, saturation and inversion in solution-state NMR [4] and in magnetic resonance imaging [5]. During a DANTE sequence, the magnetization vectors in the rotating frame undergo nutation and precession in alternation. If the offset $\Omega = \omega_0 - \omega_{rf}$ between the precession frequency of the spins ω_0 and the carrier frequency ω_{rf} coincides with a multiple of the pulse repetition rate, i.e., if $\Omega = \omega_0 - \omega_{rf} = 2\pi j/\tau_d$, with integer j, the spins precess through an

* Corresponding author. Tel.: +41 21 6939386; fax: +41 21 6933604.
E-mail address: veronika.vitzthum@epfl.ch (V. Vitzthum).
[1] Present address: Bruker BiosSpin AG, Industriestrasse 26, 8117 Fällanden, Switzerland.

1090-7807/$ - see front matter © 2012 Elsevier Inc. All rights reserved.
http://dx.doi.org/10.1016/j.jmr.2012.05.024

integer number j of full 2π rotations between two consecutive *rf* pulses. Therefore, the DANTE sequence causes the magnetization vectors to move along a meridian of the rotating frame. At other offsets, precession robs the pulses of their cumulative effect [4], so that the magnetization vectors undergo a zig-zag trajectory and remain close to the north pole. As illustrated in Fig. 1, a DANTE sequence can be described by a product of an infinite 'comb' of equidistant rectangular pulses, each of width τ_p, repeated with a period τ_d, multiplied by a boxcar function of length $K\tau_d$, where K is the total number of pulses [4]. The FT of an infinite train of Dirac delta functions with period τ_d in time domain leads to an infinite Dirac comb with intervals $1/\tau_d$ in frequency domain (Fig. 1a). The peaks in the excitation profile that occur at frequencies $\omega_{rf} + 2\pi j/\tau_d$ will be called *rf*-spikelets in the following. As a convolution in time domain is equivalent to a multiplication in frequency domain, the FT of an infinite comb of rectangular pulses of finite duration τ_p, repeated with the period τ_d, again leads to an infinite comb of Dirac *rf*-spikelets separated by $1/\tau_d$ in frequency domain, but with an envelope determined by the FT of the individual pulse, which is a sinc function with a width proportional to $1/\tau_p$ (see Fig. 1b). However, the DANTE sequence does not extend forever, since it is multiplied by a boxcar function of length $K\tau_d$. The FT of this boxcar function gives another sinc function with a width proportional to $1/(K\tau_d)$, so that each of the *rf*-spikelets is broadened accordingly (see Fig. 1c). In the examples discussed below, we have typically $\tau_p = 0.5$ μs, and hence $1/\tau_p = 2$ MHz. If we interleave N equidistant pulses per rotor period τ_{rot} to obtain a 'DANTE-N' sequence, the pulse interval is $\tau_d = \tau_{rot}/N$. For fast spinning, e.g., for $\nu_{rot} = 62.5$ kHz, one therefore obtains $\tau_d = \tau_{rot}/N = 1/(N\nu_{rot}) = 16/N$ μs. If the sequence extends over K rotor periods, the total number of pulses is NK, and the total duration $K\tau_{rot} = 160$ μs if $K = 10$, so that the width of each *rf*-spikelet is $1/(K\tau_{rot}) = \nu_{rot}/K = 6.25$ kHz. In summary, as shown in Fig. 1d, the DANTE-N excitation profile comprises a comb of *rf*-spikelets that has: (i) an

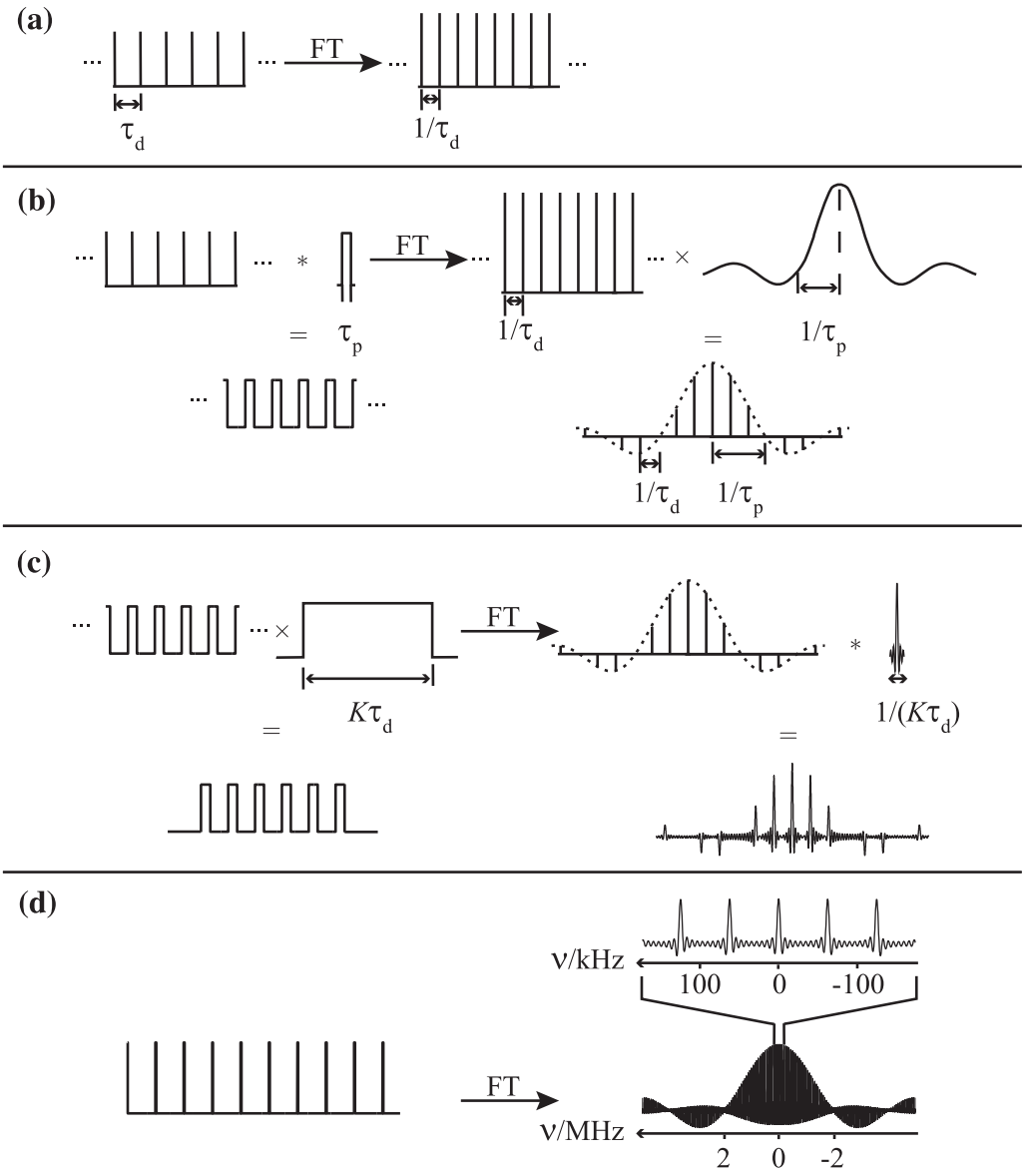

Fig. 1. Fourier transforms of an infinite comb of (a) Dirac pulses, (b) short rectangular pulses, and (c, d) finite DANTE trains of rectangular pulses of duration $\tau_p = 0.5$ μs repeated $K = 7$ times in (c) and $K = 10$ times with a period $\tau_d = 1.5$ μs in (c) and 16 μs in (d). The conditions used in (d) are appropriate for DANTE-1 at $\nu_{rot} = 62.5$ kHz. Multiplications are denoted by $\times$ and convolutions by $*$. In (c, d), $t = 0$ corresponds to the beginning of the DANTE sequence and the lengths of the first and last pulses are halved in order to obtain *rf*-spikelets in pure absorption. In (d), the frequency domain spikelets are shown over a range [−5, +5] MHz and expanded in a window of [−175, +175] kHz.

envelope with a width proportional to $1/\tau_p$ (typically 2 MHz if $\tau_p = 0.5$ μs, if we disregard bandwidth limitations due to the quality factor of the probe), (ii) a frequency interval between the spikelets equal to $N\nu_{rot}$, and (iii) each *rf*-spikelet has a width proportional to $1/(K\tau_{rot}) = \nu_{rot}/K$ (e.g., 6.25 kHz if $\nu_{rot} = 62.5$ kHz and $K = 10$). DANTE sequences may be regarded as special cases of 'tailored' excitation profiles, as discussed by Tomlinson and Hill [6].

DANTE sequences turn out to be useful in solid-state NMR of spin-1/2 nuclei, both for static samples [7], and for samples undergoing MAS [8]. In rotating solids, chemically distinct sites with different isotropic chemical shifts give rise to interlaced families of spinning sidebands that do not overlap, provided the differences in isotropic chemical shifts do not coincide with a multiple of the spinning frequency. Using a DANTE sequence with a carrier frequency ω_{rf} that coincides with the centerband (or with one of the sidebands) associated with one of the chemically distinct sites, it is possible to manipulate only one selected family of sidebands [8]. The broadband virtues of DANTE sequences have recently been rediscovered using optimal control methods [9]. Note that most applications to solids stand in contrast to selective manipulations in solution-state NMR, where one usually exploits only the central *rf*-spikelet of the DANTE spectrum, by ensuring that the other spikelets at $\omega_{rf} + 2\pi j/\tau_d$ ($j \neq 0$) fall outside the range of the spectrum.

In this work, we shall focus on 'interleaved' DANTE-*N* sequences, comprising *N* pulses per rotor period that extend over *K* rotor periods. Note that while the *K* pulses belonging to each comb must be equidistant and fulfil the condition $\tau_d = \tau_{rot} = 1/\nu_{rot}$, the *N* pulses applied within each rotor period need not be a priori equidistant. A sequence with a single pulse per rotor period ($N = 1$) will be referred to as 'basic DANTE' or 'DANTE-1'. As we shall see below, the DANTE-*N* schemes allow one to achieve efficient excitation of the magnetization of a larger fraction of crystallites than can be achieved with rectangular pulses [10–12].

With basic DANTE-1, all *K* pulses are synchronized with the rotational echoes that occur every rotor period. At the time of each rotational echo, the dephasing of magnetization components under the effect of second-rank interactions is refocused, regardless of the anisotropy of the interaction. On the other hand, the dephasing due to second-order quadrupolar interactions is not refocused since these terms do not have spatial rank $l = 2$.

In the following, we shall distinguish: (i) 'spinning sidebands' that occur at $\nu_0 + j\nu_{rot}$ (with integer *j*, including zero and negative numbers) with respect to the centerband frequency ν_0 which is determined by the sum of the isotropic chemical shift and the isotropic shift induced by the second-order quadrupole interaction, and (ii) '*rf*-spikelets' of the DANTE-*N* excitation spectrum, which occur at $\nu_{rf} + k\nu_{rot}$ (with integer *k*, including zero and negative numbers) on either side of the carrier frequency ν_{rf} (see Fig. 1).

For applications to nitrogen-14, DANTE-*N* works better and better when the spinning speed increases. Indeed, increasing ν_{rot} (i) improves the decoupling of homogeneous ^{1}H–^{1}H dipolar interactions among abundant nuclei, decreases the rotor period and hence reduces the length of the DANTE sequence. This in turn has the effect of (ii) limiting losses arising from ^{1}H–^{14}N couplings, and (iii) limiting dephasing due to second-order quadrupole effects which is not refocused by MAS.

For example, if $\nu_{rot} = 62.5$ kHz ($\tau_{rot} = 16$ μs), a DANTE-*N* sequence extending over $K = 4$ rotor periods only lasts 64 μs, regardless of *N*. The reduced overall duration increases the width of the spikelets in the *rf* excitation profile to $1/(K\tau_{rot}) = \nu_{rot}/K \approx 16$ kHz, which is quite sufficient to cover the range of isotropic chemical shifts at $B_0 = 18.8$ T (120 ppm or 9.7 kHz to cover lysine and histidine ^{14}N sites) and isotropic second-order quadrupole shifts of side-chain and backbone ^{14}N nuclei in peptides (there is a difference in second-order quadrupole shifts of 11.7 kHz between L-alanine with $C_Q = 1.14$ MHz and $\eta_Q = 0.24$, and amide sites with $C_Q = 3.2$ MHz and $\eta_Q = 0.32$). The ability to cover a broad range of offsets is beneficial not only for indirect detection [13], but also for direct excitation as shown below by recording ^{14}N signals as a function of offset.

2. DANTE-*N* sequences for direct observation

A DANTE-*N* sequence can be used to replace a simple rectangular pulse, as shown in Fig. 2. A different grey scale is used for all *K* pulses belonging to the *n*th interleaved pulse train ($n = 1,\ldots,N$). Each of the *N* pulses occurring during the first rotor period must be repeated every τ_{rot}. This requirement is mandatory in order for the *K* pulses of each of the *N* interleaved DANTE trains to be applied when the rotor has the same orientation, in order to hit the crystallites when they experience the same first-order quadrupole interactions, so that the magnetization builds up in a constructive manner. The DANTE-*N* sequence is thus comprised of *N* interleaved basic DANTE-1 sequences, which lead to *N* overlapping combs of *rf*-spikelets, all separated from the carrier frequency by multiples of the spinning frequency, $\nu_{rf} + j\nu_{rot}$. These *rf*-spikelets have phases that depend on the positions of the pulses within the rotor period. If the *n*th pulse train with an *rf* phase φ_n ($n = 1,\ldots,N$) is delayed by $\alpha_n\tau_{rot}$ ($0 \leqslant \alpha_n < 1$) with respect to the first train ($n = 1$), the *j*th *rf*-spikelet stemming from the *n*th pulse train experiences a phase shift

$$\phi_{n,j} = 2\pi j\alpha_n + \varphi_n \tag{1}$$

where *j* is an integer and φ_n is the phase of all pulses of the *n*th pulse train. One may choose to apply *N* regularly-spaced pulses in each rotor period:

$$\alpha_n = (n-1)/N \tag{2}$$

which leads to

$$\phi_{n,j} = 2\pi j(n-1)/N + \varphi_n \tag{3}$$

The combined effect of the sum of the *N* interleaved pulse trains on the complex amplitude of the *j*th spinning sideband is therefore:

$$\exp\{i\phi_j\} = \sum_{n=1}^{N}\exp\{i[2\pi j(n-1)/N + \varphi_n]\} \tag{4}$$

In the absence of any phase shifts between the different pulse trains (i.e., if φ_n is independent of *n*), the *j*th spinning sideband is *N* times more intense than with the basic DANTE-1 sequence with the same pulse length, if $j = kN$ ($k = 0, \pm1, \pm2,\ldots$) and vanishes otherwise. This comparison is only meaningful if one uses the same *K* and τ_p values. In practice however, the optimization of DANTE-1 and DANTE-*N* usually leads to different *K* and τ_p values.

The signals excited by the *rf*-spikelets thus add constructively if *j* is a multiple of *N*. The comb of spikelets of the DANTE-*N* sequence therefore only comprises frequencies $\nu_{rf} + kN\nu_{rot}$ with integer *k*. The frequency interval between neighboring spinning sidebands observed with DANTE-*N* is thus *N* times larger than with DANTE-1, as if the spinning speed was enhanced by a factor *N*. The integral of the comb of spikelets is determined by the first point of the time domain signal, which corresponds to the first pulse. Therefore, reducing the number of *rf*-spikelets entails an *N*-fold increase of the intensity of each of the remaining *rf*-spikelets.

The constructive interference of the two interleaved sequences is shown schematically in Fig. 3a–c for DANTE-2. For $n = 1$ (Fig. 3a) all spikelets have the same phase, while for $n = 2$ (Fig. 3b) their phases alternate. Their sum (Fig. 3c) leads to *rf*-spikelets that are spaced by $2\nu_{rot}$. One can achieve different interference effects by changing the *rf* phases of the pulses. If the two interleaved pulse trains have the same phases ($\varphi_1 = \varphi_2 = 0$), all spinning sidebands with an odd index *j* are cancelled out (Fig. 3d), while alternating

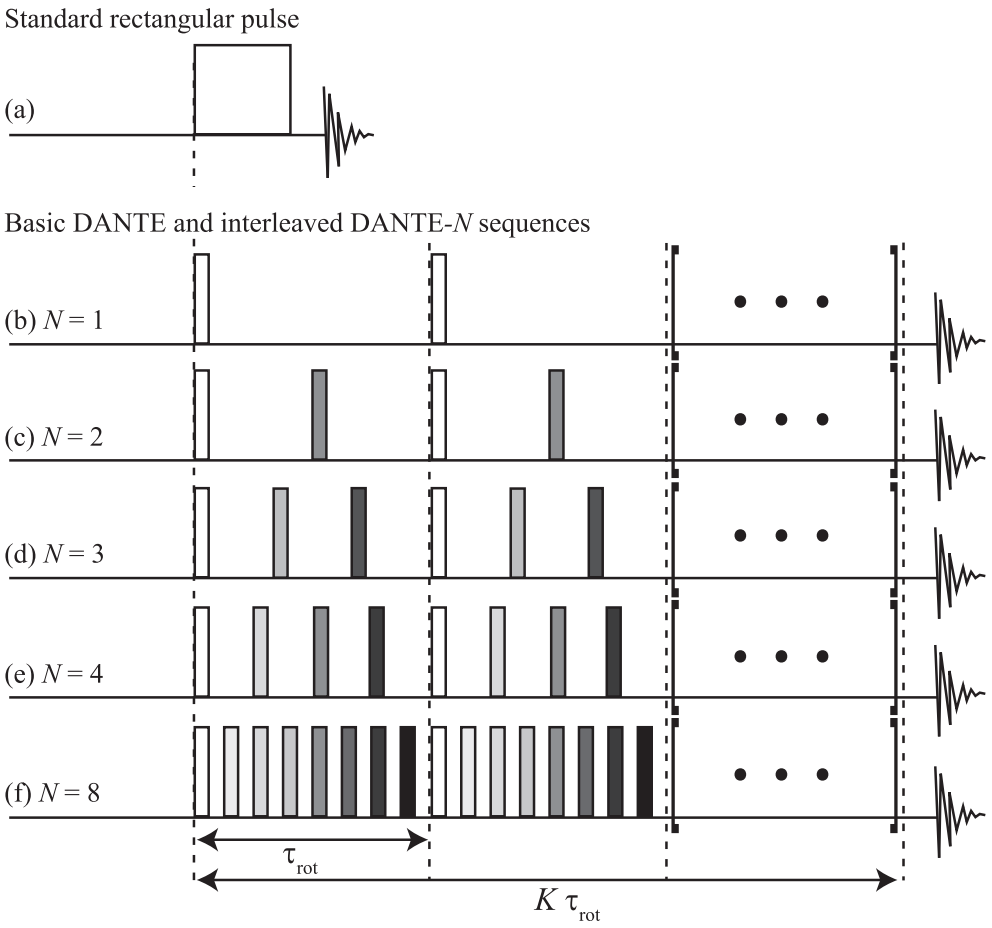

Fig. 2. Schemes for direct excitation of NMR spectra of rotating solid samples using (a) a single rectangular pulse, (b) a basic DANTE-1 sequence extending over K rotor periods with one pulse of duration τ_p per rotor period τ_{rot}, and (c–f) interleaved DANTE-N sequences with N = 2, 3, 4 or 8 equidistant pulses per rotor period, the interval between the centers of two consecutive pulses being $\tau_d = \tau_{rot}/N$. Different shades of grey correspond to the different combs n = 1, 2, ...N.

phases ($\varphi_1 = 0$ and $\varphi_2 = \pi$, i.e., $\varphi_n = (n-1)\pi$) in Eqs. (1), (3), (4) result in

$$\exp\{i\phi_j\} = 1 + \exp\{i[\pi j + \pi]\} = 1 - (-1)^j \quad (5)$$

which causes the centerband and all even sidebands to vanish (Fig. 3e).

At first sight, it might appear that the length of DANTE-N sequences, $K\tau_{rot}$, should not depend on N. In actual fact, as shown by simulations and experiments, the optimal number of rotor periods, K^{opt}, decreases as N increases, so that the total duration $K^{opt}\tau_{rot}$ of the sequence becomes shorter. This has two advantages: (i) losses due to homogeneous decay and second-order quadrupolar dephasing are reduced, and (ii) the width of the *rf*-spikelets and hence the tolerance to offsets is increased.

3. Experimental offset profiles for direct observation

While a rectangular $\pi/2$ pulse with an *rf*-amplitude ν_1 = 100 kHz and a duration τ_p = 2.5 μs can barely excite an ^{14}N spectrum over a frequency range $1/\tau_p$ = 400 kHz, a DANTE-N pulse train with τ_p = 0.5 μs can efficiently excite sidebands over a range $1/\tau_p$ = 2 MHz, limited in practice only by the Q factor of the probe. The resulting sideband patterns therefore faithfully reflect the entire breadth of the line-shape of the static sample.

It is of interest to investigate the effect of ν_{rf}, ν_1, ν_{rot}, τ_p, N and K on the envelope of the *rf*-spikelets generated by a DANTE-N sequence. To complement the offset profiles recorded previously at B_0 = 18.8 T with ν_{rot} = 31.25 kHz by rotor-synchronized indirect detection (see Fig. 4 in [13]), Fig. 4 shows experimental offset profiles for ^{14}N in γ-glycine (C_Q = 1.18 MHz and η_Q = 0.5) obtained by direct excitation at B_0 = 18.8 T with a spinning frequency ν_{rot} = 62.5 kHz.

In a first step, the pulse length τ_p has been optimized for different K and two *rf* amplitudes ν_1 = 44 kHz and 88 kHz, with the carrier frequency set on the centerband of the ^{14}N spectrum ($\nu_{rf} = \nu_0$). Then, offset profiles near the central spikelet were recorded by changing the carrier frequency over a range ν_0−5 < ν_{rf} < ν_0+5 kHz in steps of 0.4 kHz for DANTE-1 (Fig. 4a and b), and ν_0−32 < ν_{rf} < ν_0+32 kHz in steps of 4 kHz for DANTE-N (Fig. 4c and d) using either ν_1 = 44 (Fig. 4a and c) or 88 kHz (Fig. 4b and d). As explained before, the efficiency is approximately twice as large on-resonance with DANTE-2 than with DANTE-1. When K increases, the width of the *rf*-spikelets decreases as $\Delta\nu \approx 1/(K\tau_{rot})$, which corresponds to $\Delta\nu \approx$ 8.9 and 5.7 kHz for K = 7 and 11 for DANTE-1 and to $\Delta\nu \approx$ 62, 31, 21, 16, and 12 kHz for K = 1, 2, 3, 4, and 5 for DANTE-2. These predictions are qualitatively confirmed by the observations in Fig. 4. More generally, due to the smaller number K^{opt} of rotor periods, the offset profiles of the central spikelet are much broader for DANTE-N than for DANTE-1, which explains why the signals of the two nitrogen nuclei N^b and N^c of histidine are much stronger with DANTE-2 (K = 2) than with basic DANTE-1 (K = 8) in Fig. 6 of our earlier work [13].

4. Simulations of indirect detection

The DANTE-N sequences were originally shown to provide a more efficient excitation and reconversion of nitrogen-14 single-

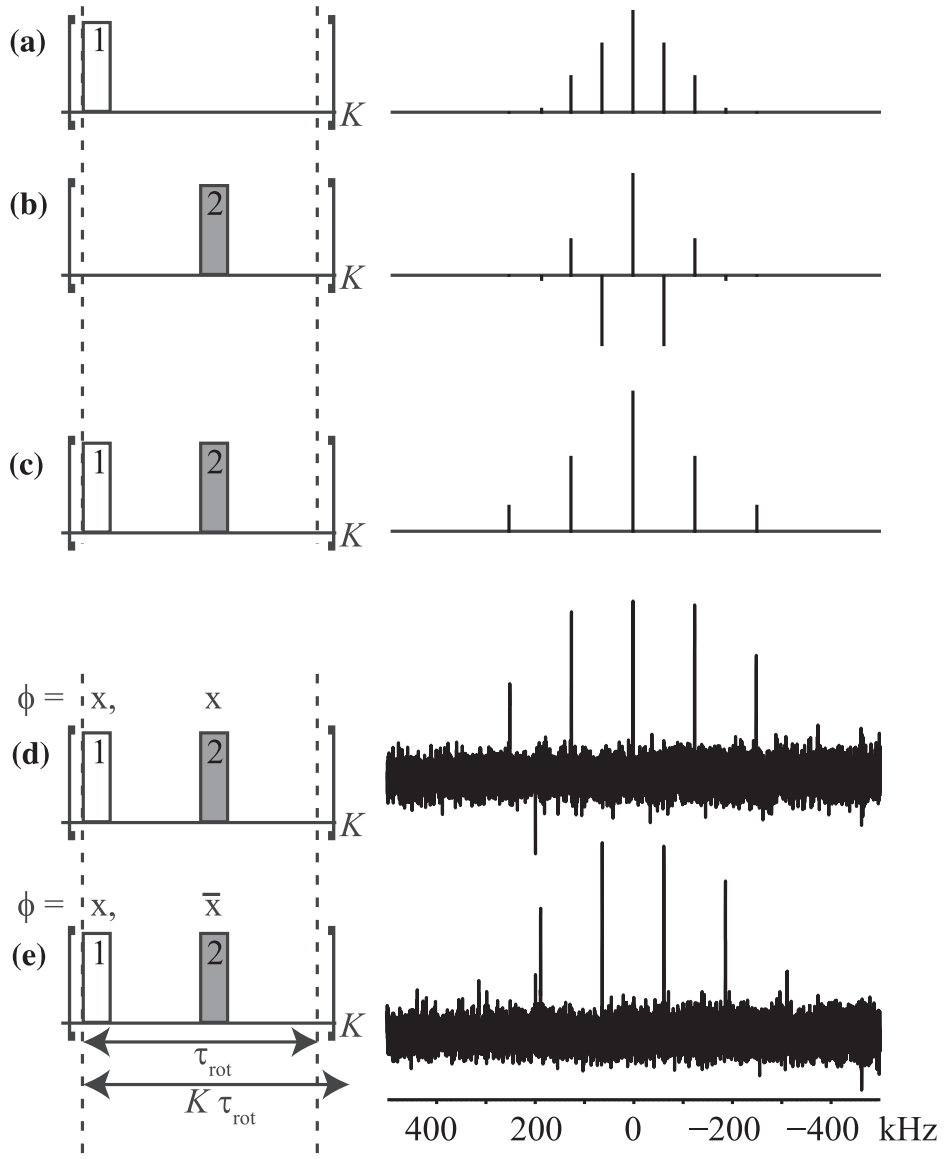

Fig. 3. (a–c) A DANTE-2 sequence can be considered as a superposition of two basic DANTE-1 sequences with $n = 1$ and 2 that are shifted in time by $\tau_{rot}/2$. This time shift induces a phase shift of $\pi j(n-1)$ for the jth spikelet in the *rf* spectrum arising from the nth comb. (a) All *rf*-spikelets associated with $n = 1$ have a common phase $\phi_{j,n=1} = 0$. (b) For the sequence with $n = 2$, the phases alternate $\phi_{n=2,j} = 0, \pi, 0, \pi, \ldots$. (c) The sum leads to the cancellation of all odd *rf*-spikelets. More generally, in the case of DANTE-*N* the superposition of *N* trains of *rf*-spikelets leads to their cancellation except for those that are separated by multiples of the spinning frequency $N\nu_{rot}$. For identical pulse lengths, the remaining *rf*-spikelets are *N* times more intense than those appearing for $N = 1$. Experimentally, the phase shifts can be observed by recording two separate ^{14}N on-resonance spectra of γ-glycine where the *rf* phases of the second comb are either $\varphi_{n=2} = 0$ (d) or $\varphi_{n=2} = \pi$ (e). In (d), only sidebands with even j survive, whereas only those with odd j appear in (e). Static field $B_0 = 18.8$ T, $\nu_{rot} = 62.5$ kHz, $\tau_{rot} = 16$ μs, $K = 2$, $\nu_1 = 88$ kHz and $\tau_p = 1.2$ μs.

and double-quantum coherences in indirect detection using ^{1}H-^{14}N-^{1}H *D*-HMQC [10–12]. Instead of standard rectangular pulses (Fig. 5a), we inserted DANTE-*N* sequences with $N = 1$, 2 or 8 (Fig. 5b, c, d) to achieve more efficient excitation and reconversion [13]. The sequences begin with the excitation of transverse magnetization of 'spy' nuclei *S*, typically ^{13}C or ^{1}H. The coherence $T^S_{1,1}$ of the 'spy' nucleus is then transformed into a superposition of coherences $T^S_{1,1}T^I_{1,0}$ and $T^S_{1,1}T^I_{2,0}$ during the first recoupling interval τ_{rec}, where the ^{1}H–^{14}N dipolar interactions are recoupled by means of a symmetry-based SR4$^2_1$ sequence [14–16]. The combination of SR4$^2_1$ sequences with high spinning frequencies allows a near-complete suppression of ^{1}H–^{1}H dipolar interactions. The ^{14}N coherence can be excited either by a rectangular pulse, or by a DANTE-*N* sequence. The ^{14}N coherence is then allowed to evolve freely during the evolution period t_1. In the middle of this period, a π pulse is applied to the ^{1}H channel. At the end of the evolution period t_1, one can again apply either a rectangular pulse or a DANTE-*N* sequence to the ^{14}N channel, in a symmetrical manner. Finally, the resulting $T^S_{1,1}T^I_{1,0}$ and $T^S_{1,1}T^I_{2,0}$ terms are converted back to coherence $T^S_{1,1}$ of the 'spy' nucleus by inserting another SR4$^2_1$ sequence during the second recoupling interval τ_{rec}. The signal of the spy nucleus is then recorded in the detection interval t_2. In conventional 2D experiments using either two rectangular pulses or two DANTE-1 sequences, the t_1 period must be incremented in integer numbers of rotor periods ($\Delta t_1 = 1/\tau_{rot}$). The use of an interleaved DANTE-*N* sequence with $N > 1$ makes it possible: (i) to multiply by *N* the spectral width in the indirect dimension, and (ii) to improve the *S*/*N* ratio [13] by oversampling in the indirect dimension [21], with increments decreasing from τ_{rot} to τ_{rot}/N. Note that one should avoid truncation and continue sampling until the signals

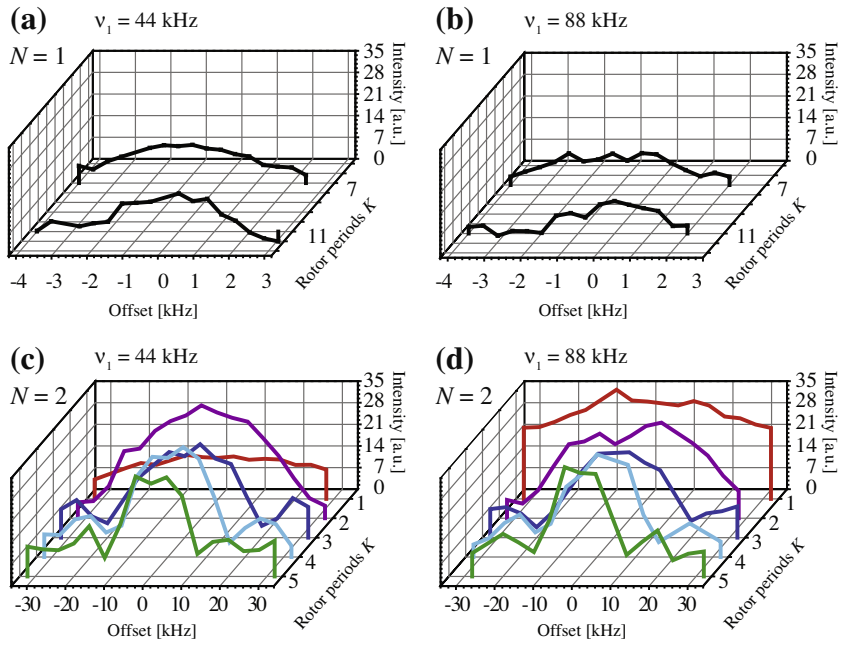

Fig. 4. Experimental signal integrals obtained by direct excitation of ^{14}N in γ-glycine as a function of the number of rotor periods K and the offset between the *rf* carrier and the centerband in the ^{14}N spectrum, recorded (a, b) with basic DANTE-1 using K = 7 or 11, and (c, d) with DANTE-2 using K = 1, 2, 3, 4 and 5, with *rf* amplitudes of ν_1 = 44 (a, c) or 88 kHz (b, d). The offset was varied in (a, b) from −5 to +5 kHz in steps of 400 Hz and in (c, d) from −32 to +32 kHz in steps of 4 kHz. Static field B_0 = 18.8 T, ν_{rot} = 62.5 kHz, τ_{rot} = 16 μs. With an *rf* amplitude ν_1 = 44 kHz, the best pulse lengths for DANTE-1 were τ_p = 1.1 and 0.7 μs for K = 7 and 11. Those for DANTE-2 were τ_p = 1.6, 1.8, 1.5, 1.0, and 0.9 μs for K = 1, 2, 3, 4 and 5, respectively. With ν_1 = 88 kHz, the best pulse lengths for DANTE-1 were τ_p = 0.8 and 0.5 μs for K = 7 and 11. Those for DANTE-2 were τ_p = 1.7, 1.1, 0.6, 0.4, and 0.4 μs for K = 1, 2, 3, 4 and 5, respectively.

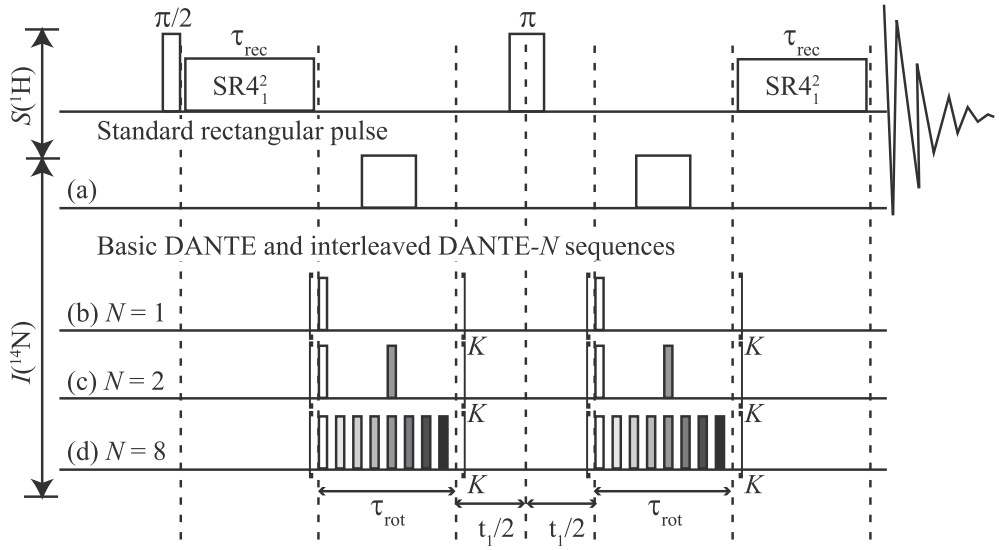

Fig. 5. Sequence for indirect detection by ^{1}H–^{14}N–^{1}H dipolar heteronuclear multiple quantum correlation (*D*-HMQC), where the ^{14}N coherences are excited and reconverted by (a) two rectangular pulses, (b–d) two DANTE-*N* sequences lasting K rotor periods with N = 1, 2 or 8. Both the pulse length τ_p and the number K of rotor periods must be optimized for each N value.

have decayed. To keep the same t_1^{max}, one obviously must record N times more increments. Non-linear sampling schemes might improve the sensitivity without sacrificing any resolution, in contrast to our earlier work [13].

Here, we compare by simulations the efficiency of the two-way transfer (^{1}H → ^{14}N → ^{1}H) obtained with square pulses (Fig. 5a) and with DANTE-1 sequences (Fig. 5b). The MATLAB simulations include scalar and dipolar couplings, and quadrupole interactions up to third order. In the simulations, we have used the quadrupolar parameters of γ-glycine (C_Q = 1.18 MHz, η_Q = 0.5) [17]. The orientation of the principal axis system of the electric field gradient (EFG) tensor with respect to the rotor frame is described by (α, β, γ) Euler angles.

The efficiency slightly depends on the angle γ, but three equidistant γ angles are sufficient to describe the powder average. In addition, we have used 615 crystallite orientations (α, β) calculated with the ZCW algorithm [18–20]. The spinning frequency was ν_{rot} = 62.5 kHz with B_0 = 18.8 T, and the carrier frequencies were set on resonance for both ^{1}H and ^{14}N nuclei.

Numerical simulations allow one to clarify the advantages achieved for indirect detection when standard rectangular pulses

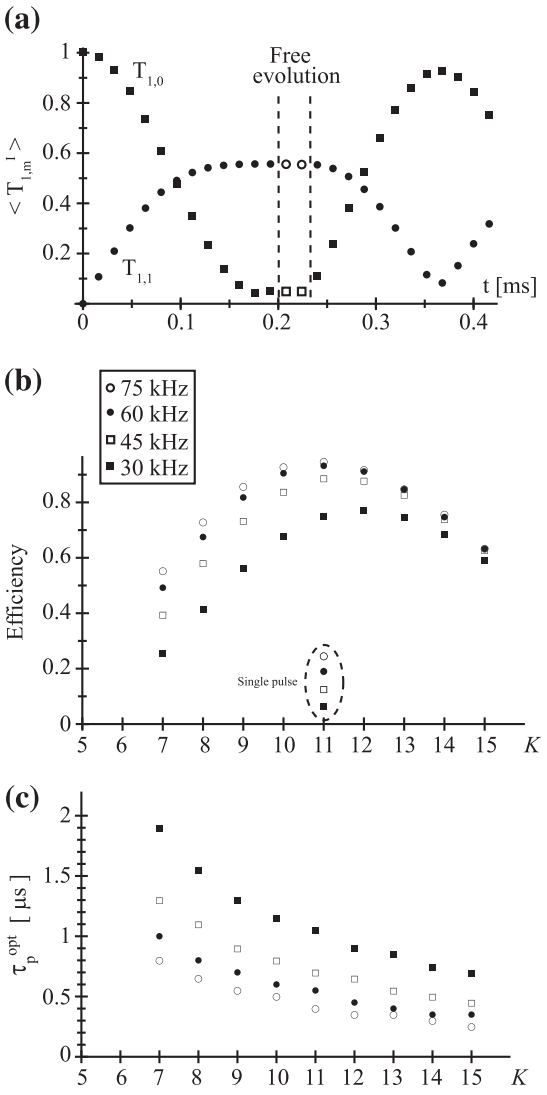

Fig. 6. Simulations of signal amplitudes that are proportional to expectation values of tensor operators obtained by indirect detection by ^{1}H-^{14}N-^{1}H *D*-HMQC for B_0 = 18.8 T, ν_{rot} = 62.5 kHz, τ_{rot} = 16 µs, ν_1 = 60 kHz and quadrupolar parameters appropriate for γ-glycine (C_Q = 1.18 MHz, η_Q = 0.5) using integrations over 615 crystallite orientations (α, β). Only first-rank excitation and inter conversion processes $T^l_{1,0} \leftrightarrow T^l_{1,1}$ were considered. (a) Expectation values of single-quantum nitrogen coherences $T^l_{1,1}$ after K = 1, 2, ..., 12 pulses of duration τ_p = 0.55 µs of a basic DANTE-1 sequence, calculated after integer rotor periods. The first-rank Zeeman populations $T^l_{1,0}$ (filled squares) decrease while single-quantum nitrogen coherences $T^l_{1,1}$ (filled dots) build up. Each pulse thus contributes to the excitation of coherences in a constructive manner. The subsequent free evolution interval (open squares and dots) lasts two rotor periods ($t_1 = 2\tau_{rot}$). The second burst of DANTE-1 pulses reconverts the nitrogen coherences $T^l_{1,1}$ back to populations $T^l_{1,0}$, again in a constructive way. (b) Excitation-reconversion efficiency of ^{1}H-^{14}N-^{1}H (considering the two-step conversion $T^l_{1,0} \rightarrow T^l_{1,\pm1} \rightarrow T^l_{1,0}$) for *D*-HMQC as a function of the number of rotor periods K used in a symmetrical fashion for each of the two basic DANTE-1 sequences, considering pulses of length τ_p = 0.4 µs with four different *rf* amplitudes ν_1 = 30, 45, 60 and 75 kHz. The four symbols emphasized by a dashed ellipse show the efficiency for two standard rectangular pulses of duration τ_p = 4.4 µs < τ_{rot} = 16 µs, i.e., with the same total duration as K = 11 pulses lasting 0.4 µs each. (c) Optimum pulse durations τ_p^{opt} that allow one to achieve the best efficiency of the two-step conversion $T^l_{1,0} \rightarrow T^l_{1,\pm1} \rightarrow T^l_{1,0}$ for different K values and amplitudes ν_1 = 30, 45, 60 and 75 kHz, using the same symbols as in (b).

are replaced by DANTE sequences. The constructive character of the DANTE-1 sequence is illustrated by the simulations in Fig. 6a, which show the magnitudes of longitudinal ^{14}N magnetization, represented by the Zeeman tensor operator $T^l_{1,0}$ (full squares) [17], and of first-rank single-quantum coherences $T^l_{1,1}$ (full dots). These terms are excited by applying one pulse per rotor period with an *rf*-amplitude ν_1 = 60 kHz and a pulse length τ_p = 0.55 µs. We clearly observe that every pulse contributes constructively to the coherence $T^l_{1,1}$ while the initial longitudinal magnetization $T^l_{1,0}$ is gradually depleted. We have used K = 12, the optimum transfer being observed for K^{opt} = 11 (see Fig. 6b), where one notices a quasi-ideal conversion of $T^l_{1,0}$ into $T^l_{1,1}$, as for a perfect π/2 rotation of the ^{14}N magnetization. The simulations show that the creation of $T^l_{1,1}$ during the first DANTE-1 sequence does not follow a sinusoidal pattern as would be expected for a Rabi nutation, but reaches a flat maximum. The subsequent free evolution period t_1, which is equal to $2\tau_{rot}$ in Fig. 6a, is represented by empty squares and dots. A second DANTE-1 sequence is then applied to the ^{14}N spins, leading to the reconversion of coherences $T^l_{1,1}$ into populations $T^l_{1,0}$. The evolution of the density operator during the two SR4$^2_1$ recoupling intervals was not taken into account in the simulations. This approximation is justified in ultra-fast MAS where the rotor periods are short so that losses are minimized, but second-order quadrupole interactions, homogeneous decay and relaxation play an increasing role if the number of rotor periods increases or if the spinning frequency is slowed down.

The excitation-reconversion efficiency of the DANTE-1 sequences in *D*-HMQC experiments (Fig. 5b with t_1 = 0) is illustrated in Fig. 6b for *rf* amplitudes ν_1 = 30, 45, 60, 75 kHz as a function of the number K of rotor periods. In these simulations, the pulse length was fixed to τ_p = 0.4 µs, which is the optimal value for ν_1 = 75 kHz and K^{opt} = 11 (Fig. 6c). The optimal number of rotor periods does not have a pronounced dependence on the *rf*-amplitude, i.e., K^{opt} = 11 for 45 < ν_1 < 75 kHz and K^{opt} = 12 for ν_1 = 30 kHz. For $K \geqslant 14$, the efficiencies are similar regardless of the *rf*-amplitude. Similarly, for K^{opt} = 11, the cumulative flip angle, corresponding to the sum of all K^{opt} pulses each of duration τ_p, is θ_{tot} = 71° for ν_1 = 45 kHz, θ_{tot} = 95° for ν_1 = 60 kHz and θ_{tot} = 119° for ν_1 = 75 kHz. Nevertheless, the efficiency only increases slightly from ν_1 = 45 to 75 kHz. This is in agreement with the broad maximum of Fig. 6a. The highest efficiency is obtained for cumulative flip angles 70° < θ_{tot} < 120°. Thus if τ_p = 0.4 µs, ν_1 = 75 kHz and K^{opt} = 11, one obtains $\theta_{tot} \approx 120°$. The efficiency achieved using standard rectangular pulses with various *rf*-amplitudes was also calculated using a total pulse length $K^{opt}\tau_p$ = 4.4 µs, which corresponds to the sum of all pulses in a DANTE-1 sequence with K^{opt} = 11 and τ_p = 0.4 µs (see points enclosed by a dashed circle in Fig. 6b). For the same total area of the *rf* pulses, the DANTE-1 sequence leads to a four-fold boost of efficiency compared to standard rectangular pulses.

Thus the use of basic DANTE-1 sequences leads to more efficient excitation and reconversion than standard rectangular pulses. Experimental comparisons between rectangular pulses and

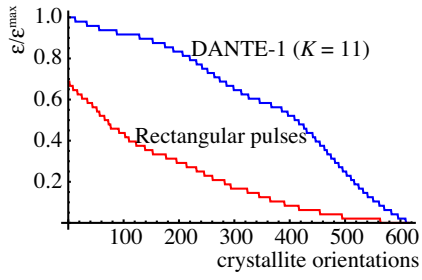

Fig. 7. Normalized excitation-reconversion efficiency $\varepsilon/\varepsilon^{max}$ of the two-step conversion $T^l_{1,0} \rightarrow T^l_{1,\pm1} \rightarrow T^l_{1,0}$ in *D*-HMQC for the same 615 distinct crystallite orientations (α, β) as in the simulations of Fig. 6. The number of orientations is sorted according to the efficiency. The parameters correspond to B_0 = 18.8 T, ν_1 = 60 kHz, ν_{rot} = 62.5 kHz, C_Q = 1.18 MHz, η_Q = 0.5. The top curve shows the statistics when using two DANTE-1 sequences (τ_p^{opt} = 0.55 µs, K^{opt} = 11), and the bottom curve when using two rectangular pulses of duration τ_p = 20 µs.

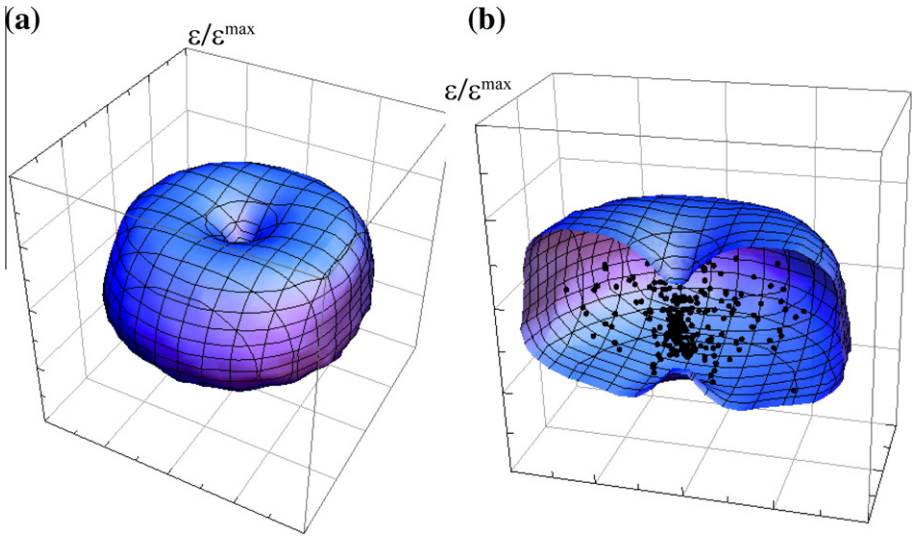

Fig. 8. Normalized excitation-reconversion efficiency $\varepsilon/\varepsilon^{max}$ of the two-step conversion $T^I_{1,0} \rightarrow T^I_{1,\pm1} \rightarrow T^I_{1,0}$ in *D*-HMQC for integrals over 615 crystallite orientations (α, β) with B_0 = 18.8 T, ν_1 = 60 kHz, ν_{rot} = 62.5 kHz, τ_{rot} = 16 μs, C_Q = 1.18 MHz, η_Q = 0.5. (a) Relative efficiencies using DANTE-1 with τ_p = 0.55 μs and K^{opt} = 11, represented by vectors with lengths $\varepsilon/\varepsilon^{max}$ and polar angles (α, β). These vectors span a surface with the shape of a 'doughnut', with an efficiency that is high near the equator but drops near the poles. (b) Exploded view of (a), where the dots represent the apparently erratic efficiencies $\varepsilon/\varepsilon^{max}$ of the excitation and reconversion of the same 615 crystallites if one uses two rectangular pulses of duration τ_p = 20 μs while τ_{rot} = 16 μs.

DANTE-*N* sequences show that for fast MAS ($\nu_{rot} \geqslant 60$ kHz) significant sensitivity improvements are indeed observed [13]. At moderate spinning speeds ($30 < \nu_{rot} < 35$ kHz), the advantages are less significant.

Fig. 6c demonstrates that the optimum pulse length τ_p^{opt} is always inversely proportional to *K* and that the cumulative flip angle is always in the range $70° < \theta_{tot} < 120°$. The increased efficiency of *D*-HMQC using DANTE-*N* sequences rather than rectangular pulses can be ascribed to the larger number of crystallite orientations that are efficiently excited. To confirm this hypothesis, further simulations were carried out to investigate the excitation and reconversion efficiency as a function of the crystallite orientations. The experimental parameters were ν_1 = 60 kHz, $\tau_p^{opt} = 0.55$ μs, K^{opt} = 11, and the carrier frequency was set on resonance. Fig. 7 represents the relative efficiency $\varepsilon/\varepsilon^{max}$ of the two-way transfer ($^1H \rightarrow {}^{14}N \rightarrow {}^1H$) in *D*-HMQC as a function of the crystallite orientations, ranked in decreasing order. Two histograms are shown, one for DANTE-1 sequences and one for rectangular pulses. The DANTE-1 scheme leads both to a higher overall efficiency and to a more uniform excitation of the crystallites.

In order to depict the uniformity of the excitation that can be achieved with the DANTE-1 scheme, the relative efficiency $\varepsilon/\varepsilon^{max}$ associated with various crystallite orientations has been represented in Fig. 8 by a vector with polar angles (α, β) and a modulus proportional to $\varepsilon/\varepsilon^{max}$, where ε^{max} is the maximum achievable efficiency. The *z*-axis in the figure corresponds to crystallites where the V_{zz} component of the EFG tensor is aligned with the rotor axis. For DANTE-1 sequences, the spatially uniform distribution of the vectors allows one to fit their extremities with a 3D surface that resembles a 'doughnut'. Note that the efficiency is close to one near the equator and dips in the vicinity of the poles. The efficiency decreases if the quadrupole interaction increases.

For rectangular pulses, the erratic efficiencies are represented by red dots that do not lie on a smooth surface (Fig. 8b), thus confirming the haphazard distribution of crystallite orientations excited by rectangular pulses. This chaotic behavior is due to the lengths of the two rectangular pulses (τ_p = 20 μs each) while τ_{rot} = 16 μs. The fluctuating quadrupole interactions are too large during a fraction of the rotor cycle for the *rf* pulses to be effective. This is not the case for DANTE-1 sequences, which only use very short pulses.

Simulations of DANTE-1 sequences combined with ^1H–^{14}N–^1H *D*-HMQC experiments have been performed for various quadrupole interactions. They show that the optimum pulse length τ_p^{opt} that allows one to excite all crystallites uniformly is inversely proportional to C_Q and that the optimum number of rotor periods K^{opt} must be proportional to C_Q in order to obtain a cumulative flip angle $70° < \theta_{tot} < 120°$. However, it must be remembered that these simulations do not take into account homogeneous losses and bandwidth limitations due to the quality factor *Q* of the probe.

5. Conclusions

We have analyzed and compared signal intensities of ^{14}N spectra ($I = 1$) with quadrupole interactions of several MHz in samples that are spinning about the magic angle. The ^{14}N coherences have been excited with rectangular pulses, basic DANTE-1 and interleaved DANTE-*N* sequences ($N > 1$). Comparisons have been made not only for experimental ^{14}N spectra observed by direct detection, but also for simulations of indirect ^1H–^{14}N–^1H *D*-HMQC experiments. We have shown that with very fast spinning, a significant increase in sensitivity can be obtained with DANTE-*N* sequences compared to rectangular pulses, owing to the much larger number of crystallite orientations that can be excited efficiently. The main limitation of the basic DANTE-1 sequence lies in its sensitivity to offsets, which may hinder applications to samples that contain several ^{14}N nuclei with very different isotropic chemical shifts or second-order quadrupole interactions. This limitation can be overcome with DANTE-*N* sequences ($N > 1$), which may be combined with non-linear oversampling of the signal in the indirect dimension of 2D experiments, thus providing a significant gain in sensitivity.

Acknowledgments

This work was supported by the Swiss National Science Foundation (SNSF), the Swiss Commission for Technology and Innovation

(CTI), and by the Fédération de Recherche (FR-3050) Très Grands Equipements de Résonance Magnétique Nucléaire à Très Hauts Champs (TGIR RMN THC) supported by the French CNRS. Julien Trébosc, Olivier Lafon, and Jean-Paul Amoureux are grateful for funding provided by Région Nord/Pas de Calais, the European Union (FEDER), the CNRS, the French Ministry of Scientific Research, USTL, ENSCL, CortecNet and Bruker Biospin. This work was supported by contract ANR-2010-jcjc-0811-01.

References

[1] R.R. Ernst, W.A. Anderson, Application of Fourier transform spectroscopy to magnetic resonance, Rev. Sci. Instrum. 37 (1966) 93–102.
[2] L.A. O'Dell, R.W. Schurko, K.J. Harris, J. Autschbach, C.I. Ratcliffe, Interaction tensors and local dynamics in common structural motifs of nitrogen: a solid-state ^{14}N NMR and DFT study, J. Am. Chem. Soc. 133 (2011) 527–546.
[3] G. Bodenhausen, R. Freeman, G.A. Morris, A simple pulse sequence for selective excitation in Fourier transform NMR, J. Magn. Reson. 23 (1976) 171–175.
[4] G.A. Morris, R. Freeman, Selective excitation in Fourier transform nuclear magnetic resonance, J. Magn. Reson. 29 (1978) 433–462.
[5] T.R. Saarinen, C.S. Johnson, Imaging of transient magnetization gratings in NMR. Analogies with laser-induced gratings and applications to diffusion and flow, J. Magn. Reson. 78 (1988) 257–270.
[6] B.L. Tomlinson, H.D.W. Hill, Fourier synthesized excitation of nuclear magnetic resonance with application to homo-nuclear decoupling and solvent line suppression, J. Chem. Phys. 59 (1973) 1775–1784.
[7] D.E. Wemmer, E.K. Wolff, M. Mehring, Multiple-frequency excitation (MFE) a technique for observing broad-line transients, J. Magn. Reson. 42 (1981) 460–473.
[8] P. Caravatti, G. Bodenhausen, R.R. Ernst, Selective pulse experiments in high-resolution solid state NMR, J. Magn. Reson. 55 (1983) 88–103.
[9] M. Bjerring, B. Paaske, H. Oschkinat, U. Akbey, N.C. Nielsen, Rapid solid-state NMR of deuterated proteins by interleaved cross-polarization from ^{1}H and ^{2}H nuclei, J. Magn. Reson. 214 (2012) 324–328.
[10] Z. Gan, Measuring amide nitrogen quadrupolar coupling by high-resolution ^{14}N/^{13}C NMR correlation under magic-angle spinning, J. Am. Chem. Soc. 128 (2006) 6040–6041.
[11] S. Cavadini, A. Lupulescu, S. Antonijevic, G. Bodenhausen, Nitrogen-14 NMR spectroscopy using residual dipolar splittings in solids, J. Am. Chem. Soc. 128 (2006) 7706–7707.
[12] S. Cavadini, S. Antonijevic, A. Lupulescu, G. Bodenhausen, Indirect detection of nitrogen-14 in solid-state NMR spectroscopy, ChemPhysChem 8 (2007) 1363–1374.
[13] V. Vitzthum, M.A. Caporini, S. Ulzega, G. Bodenhausen, Broadband excitation and indirect detection of nitrogen-14 in rotating solids using delays alternating with nutation (DANTE), J. Magn. Reson. 212 (2011) 234–239.
[14] J. Trébosc, B. Hu, J.P. Amoureux, Z. Gan, Through-space R3-HETCOR experiments between spin-1/2 and half-integer quadrupolar nuclei in solid-state NMR, J. Magn. Reson. 186 (2007) 220–227.
[15] A. Brinkmann, A.P.M. Kentgens, Proton selective ^{17}O–^{1}H distance measurement in fast magic-angle-spinning solid-state NMR spectroscopy for the determination of hydrogen bond length, J. Am. Chem. Soc. 128 (2006) 14758–14759.
[16] B. Hu, J. Trébosc, J.P. Amoureux, Comparison of several hetero-nuclear dipolar recoupling NMR methods to be used in MAS HMQC/HSQC, J. Magn. Reson. 192 (2008) 112–122.
[17] S. Cavadini, Indirect detection of nitrogen-14 in solid-state NMR spectroscopy, Prog. NMR Spectrosc. 56 (2010) 46–77.
[18] V.B. Cheng, H.H. Suzukawa, M. Wolfsberg, Investigations of a non-random numerical method for multi-dimensional integration, J. Chem. Phys. 59 (1973) 3992–3999.
[19] H. Conroy, Molecular Schrodinger equation. VIII. A new method for evaluation of multi-dimensional integrals, J. Chem. Phys. 47 (1967) 5307–5318.
[20] S. Zaremba, Good lattice points, discrepancy, and numerical integration, Ann. Mat. Pur. Appl. 73 (1966) 293–317.
[21] O. Lafon, B. Hu, J.P. Amoureux, P. Lesot, Fast and high-resolution stereo-chemical analysis by non-uniform sampling and covariance processing of anisotropic NAD NMR 2D data, Chem. Eur. J. 17 (2011) 6716–6724.